Simultaneous energy distribution and ion fraction measurements using a linear time-of-flight analyzer with a floatable drift tube

V. A. Morozov and F. W. Meyer
Physics Division, Oak Ridge National Laboratory, Oak Ridge, Tennessee 37831-6372

(Received 15 June 1999; accepted for publication 30 August 1999)

A technique for simultaneous energy distribution and ion fraction measurements using a linear time-of-flight analyzer with a floatable drift tube is described. Analytical expressions for the relative collection efficiency and viewing region of the apparatus are developed as functions of the analyzed particle reduced energy and dimensionless apparatus parameters. The method was applied to studies of large-angle scattering of singly charged oxygen ions incident on Au(110), and carried out at the Oak Ridge National Laboratory's Multicharged Ion Research Facility. Energy distributions of the scattered projectiles and the negative ion fraction are presented as a function of scattered projectile energy. As a by-product of the measurements, the relative ion detection efficiency of the particle detector was reconstructed as a function of ion impact energy on the detector. © *1999 American Institute of Physics.*[S0034-6748(99)02112-7]

I. INTRODUCTION

Time-of-flight (TOF) particle analysis is a well known experimental technique that requires no special introduction. Its most popular application is in the area of mass spectrometry where its capability of delivering complete mass spectra with high speed and sensitivity makes possible analysis of species ranging from light molecular and atomic species to huge biomolecules.[1,2] Even though the energy resolution of a typical TOF apparatus is typically poorer than that of electrostatic energy analyzers, the TOF technique is widely used in energy loss analysis and is often the only means available for measuring energy distribution of neutral particles.[3,4] The latter feature is of particular value in ion–surface scattering experiments, since a significant fraction of the scattered particles are neutrals.

In combination with the less used ''voltage labeling technique,''[5,6] TOF analysis allows simultaneous measurement of the neutral as well as scattered ion fractions. Voltage labeling consists of the time separation of charged particles on the basis of their different kinetic energy gains in regions of nonzero electrostatic field. After appropriate TOF-to-energy transformation the detected particle energy distributions $n_q(E)$ can be obtained. These distributions are related to the true particle energy distributions $N_q(E)$ through the relation $n_q(E)=N_q(E)\times F(E,qU)\times D(E_d,q)$, where $F(E,qU)$ defines the collection efficiency of the apparatus (i.e., the fraction of particles with charge q and energy E entering the analyzer and eventually reaching the detector when voltage U is applied to the drift tube), and $D(E_d,q)$ is the detector efficiency depending in general on particle impact kinetic energy on the detector $E_d=E+qV$ (V is the potential on the front of the detector) and charge q. When functions F and D are known, the ion fractions can be determined. In the simplest case where a singly charged and a neutral component dominate the projectile flux to be analyzed, the ion fraction is given by

$$\frac{N_q}{N_q+N_0}=\frac{1}{1+\dfrac{n_0(E)}{n_q(E)}\times\dfrac{F(E,qU)}{F(E,0)}\times\dfrac{D(E+qV,q)}{D(E,0)}}. \quad (1)$$

The first ratio in the denominator of expression (1) is directly measured, while the second one depends on the apparatus design and can be calculated. With regard to the third ratio, determination of even relative detection efficiencies for ions and neutrals is usually a very difficult experimental task. However, for the comparatively high kinetic energies (~1 keV and above) needed in many cases to detect neutrals, it can be simplified by the reasonable assumption that the detection efficiency of typically used secondary electron multipliers does not depend on particle charge state[7,8] (i.e., that secondary electron emission in this energy range has mainly a kinetic origin). This transforms the ratio required into a ratio of ion detection efficiencies for two different ion detector impact energies, the first being that of the (accelerated) ion and the second equaling that of the corresponding neutral. The ion impact energy can be easily changed by varying the drift tube voltage (and keeping the same all other detector voltages referenced to it to maintain identical detection conditions). This means, in general, making auxiliary measurements at lower ion energy E' for two different drift tube voltages, and hence two detector face potentials V' and V'' such that $E'+qV'=E$ and $E'+qV''=E+qV$ in expression (1), but the experimental conditions (e.g., incidence angle, target azimuth, scattering angle, etc. in ion–surface scattering) of these measurements can be chosen for the maximum ion count rate. Of course, decelerating the ions back to their original energy (i.e., making them isoenergetic with the scattered neutrals) prior to detection by setting the potential on the front detector face to zero eliminates the need for the latter step [since it would make the third factor in the denominator of expression (1) identically equal to unity], but this is not always the best solution. The ion detection efficiency may drop dramatically with decreasing impact en-

ergy, and, if the ion fraction is small, this means long acquisition times to get sufficiently good statistics. As will be shown, implementation of a floatable drift tube permits direct measurement of this ratio and allows the detector face to be kept at nonzero potential in order to ensure high ion detection efficiency. Analysis of the ion TOF spectra recorded for different tube voltages also makes possible extraction of more detailed information about the relative ion detection efficiency $D(E_d)$ itself as a function of ion detection energy, which can be useful for many applications.

Compared with other techniques used for ion fraction measurements, this method does not require the long acquisition times, needed, e.g., when the ion fraction is obtained by subtracting the neutral spectra from corresponding spectra of neutrals and ions,[8,9] and has the advantage of simplicity of design (no moving parts, a single conventional detector instead of the more complicated position sensitive detectors,[4,7] or multidetector systems[10] required when neutrals and ions are separated by passage through a region of transverse electrostatic field). Information about energy distributions and scattered ion charge fractions gained by any of the above means often provides important clues for understanding the physical mechanisms involved in the interaction being studied.

II. MAIN FEATURES OF LINEAR TOF MEASUREMENTS WITH A FLOATABLE DRIFT TUBE

The geometry of a linear TOF analyzer with a floatable drift tube is shown in Fig. 1. For the sake of simplicity the regions of nonzero electric field (linear acceleration regions between sections and in front of the detector) are ignored. Considering a beam of particles with mass m, charge q, and energy E traveling close to the apparatus axis ($\alpha,\beta \ll 1$) the flight time in such a system is given by

$$T=\sqrt{\frac{m}{2}}\times\left(\frac{l}{\sqrt{E}}+\frac{L}{\sqrt{(E+|qU|)}}\right), \tag{2}$$

where acceleration voltage U is applied to the drift tube (the deceleration mode is less common since in that case the ion peaks are typically broader and sit on top of the neutral tail).

Two features of the analyzer are highlighted. First, due to the finite size of the detector, the collection efficiency depends obviously on the particle charge state. As can be seen from Fig. 1, assuming a point source on the TOF axis, only those neutrals whose trajectories are enclosed in circle b can be detected, while for ions the corresponding circle, c, is larger. Using the equality $R=\nu_\perp T$, the perpendicular velocity $\nu_\perp$ for the particle's extreme trajectory reaching the detector at radius R (see Fig. 1) can be determined; the radius of the corresponding circle in the plane separating the zero and nonzero drift tube voltage regions is given by

$$r=\nu_\perp t=\frac{R}{T}t=\frac{Rk_0}{k_0+[1/\sqrt{1+(1/\epsilon)}]}, \tag{3}$$

where $t=l/\sqrt{(2E/m)}$ is the particle flight time in the field-free region, $k_0=l/L$ is one of the analyzer parameters and $\epsilon=|E/qU|$ is the particle reduced energy ($1/\epsilon=0$ for neutrals). The relative collection efficiency, defined now as the ratio of the number of ions and equivalent neutrals from a point source that strikes the detector, is given by

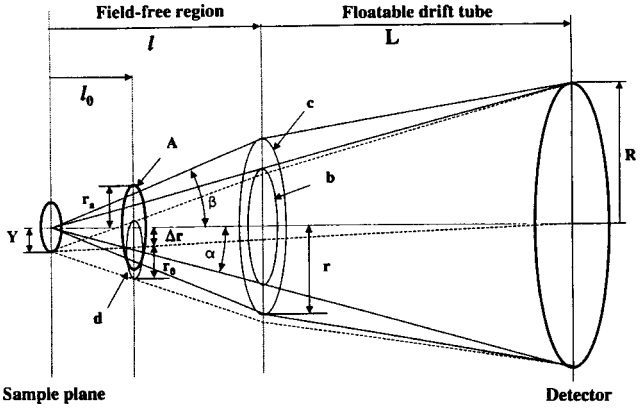

FIG. 1. Geometrical diagram of the linear TOF analyzer with a floatable drift tube, consisting of two field-free sections of length l and L with potential difference U between them. Aperture A is the smallest angular acceptance aperture of the apparatus.

$$f_{\rm ps}(\epsilon)=\frac{F(E,qU)}{F(E,0)}=\frac{S_c}{S_b}=\left(\frac{1+k_0}{k_0+[1/\sqrt{1+(1/\epsilon)}]}\right)^2, \tag{4}$$

where S_b and S_c are the areas of circles b and c, respectively.

Considering now trajectories originating at some distance Y from the apparatus axis (i.e., assuming an extended source), it may be seen from Fig. 1 that not all trajectories terminating on the detector surface in fact pass through the aperture of the TOF system, A. Note that since all angles are small, the radius of circle d to first approximation does not depend on Y and is given by $r_0=r\times l_0/l$, where l_0 is the position of aperture A. Since r_0 depends (through r) also on reduced energy, the viewing region of the TOF system is defined not only by its geometry but also by ϵ. The fraction of particles $g(Y)$ which are actually detected is defined by the overlap of circle d with aperture A. After adopting the following variable and parameter definitions (see Fig. 1),

$$p=\frac{r_0}{r_a}=\frac{k_1k_2}{k_0+1/\sqrt{1+(1/\epsilon)}},$$

$$x=\frac{\Delta r}{r_a}=\frac{Y}{r_a}\frac{1+k_0-k_2}{1+k_0},\quad y=\frac{Y}{r_a},$$

with $k_1=R/r_a$, $k_2=l_0/L$ as two additional dimensionless apparatus parameters, a straightforward derivation, omitted here, shows that the fraction $g(y)$ is given by

$$g(y)=\begin{cases}1; & x<1-p\\ 0; & x>1-p\\ 1-\dfrac{1}{\pi}\left\{\arccos\left(\dfrac{1-p^2-x^2}{2px}\right)-\dfrac{1}{p^2}\left[\arccos\left(\dfrac{1-p^2+x^2}{2x}\right)-\dfrac{\sqrt{[p^2-(x-1)^2][(x+1)^2-p^2]}}{2}\right]\right\} & \\ 1-p\leqslant x\leqslant 1+p,\end{cases} \tag{5a}$$

for the case of $r_0\leqslant r_a (p\leqslant 1)$ and

$$g(y)=\begin{cases}1, & x<p-1,\\ 0, & x>p-1,\\ \dfrac{1}{p^2}\left\{1-\dfrac{1}{\pi}\left[\arccos\left(\dfrac{p^2-1-x^2}{2x}\right)-p^2\arccos\left(\dfrac{p^2+x^2-1}{2px}\right)-\dfrac{\sqrt{[1-(x-p)^2][(x+p)^2-1]}}{2}\right]\right\}, & \\ p-1\leqslant x\leqslant p+1.\end{cases} \tag{5b}$$

for the case of $r_0>r_a (p>1)$.

As an illustration several ''viewing region'' curves for our particular apparatus are shown in Fig. 2. The total number of detected particles of given energy is defined by the integral $n(\epsilon)=N(E)\int s(y)g(y,\epsilon)dy$, where $N(E)$ and $s(y)$ are the beam energy distribution and beam intensity profile, respectively. The results of numerical integration of this expression assuming several Gaussian-shaped beam profiles of different widths, w, are shown in Fig. 3. As can be seen, when taking into account finite beam size (i.e., assuming an extended source), the effective ion transmission of the apparatus is reduced beyond critical values of the inverse reduced energy that depend on the beam width w. The relative collection efficiency, expression (4), therefore has to be modified to

$$f_{\rm es}(\epsilon)=f_{\rm ps}(\epsilon)\times\frac{\int s(y)g(y,1/\epsilon)dy}{\int s(y)g(y,0)dy}. \tag{6}$$

The dependence of point-source and extended-source relative collection efficiencies on reduced particle energy is shown in Fig. 4 as lines for two different beam profiles together with results $f_{\rm sim}$ (shown by symbols for one of the assumed beam profiles) of a simulation that takes into account flight times in all regions of the apparatus (i.e., with all nonzero electric field regions included). As can be seen, good agreement (the relative error is less than 5%) is found over the whole range of reduced energies.

Turning now to the second feature of TOF measurements with a floatable drift tube, it can be shown by taking the derivative of expression (1) that the simple relation between relative energy and time of flight errors $\Delta E/E=2\Delta t/t$, valid for standard linear TOF systems, has to be replaced by

$$\frac{\Delta E}{E}=\frac{\Delta t}{t}\times S(k_0,\epsilon),$$

where

$$S(k_0,\epsilon)=\frac{2}{1-1/[(1+\epsilon)(1+k_0\sqrt{1+(1/\epsilon)})]}. \tag{7}$$

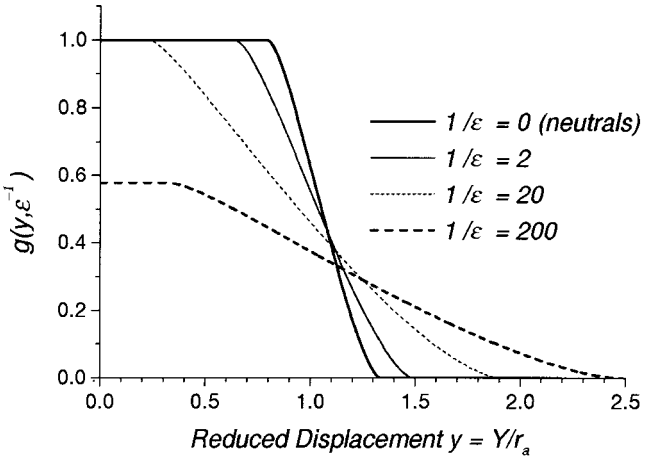

FIG. 2. Viewing region curves $g(y,\epsilon^{-1})$ for the linear TOF apparatus with a floatable drift tube and with a particular set of dimensionless parameters: $k_0=0.15$; $k_1=4.2$; $k_2=0.068$ [see the text and expression (5) for definitions; $\epsilon^{-1}=|qU/E|$ is the inverse reduced energy].

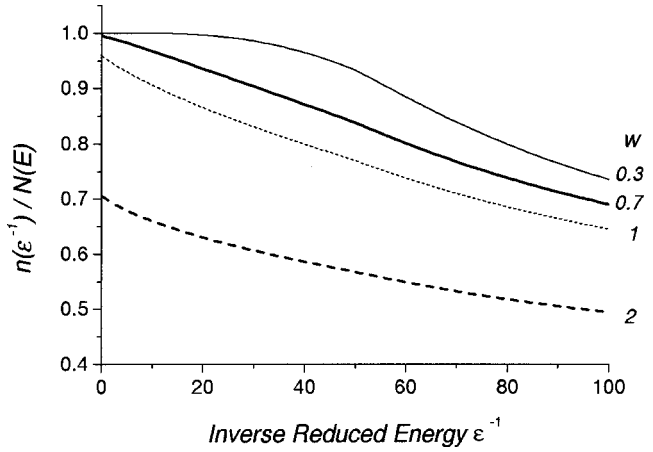

FIG. 3. Ratio of the number of detected particles $n(\epsilon)$ to the total number of particles $N(E)$ of given energy E entering the analyzer whose viewing region curves are presented in Fig. 2 as a function of the inverse reduced energy $\epsilon^{-1}=|qU/E|$ for several Gaussian-shaped beam profiles $s(y)=(\sqrt{2/\pi}/w)\exp[-2(y/w)^2]$ (width, w, is in units of r_a, the radius of the smallest angular acceptance aperture of the apparatus).

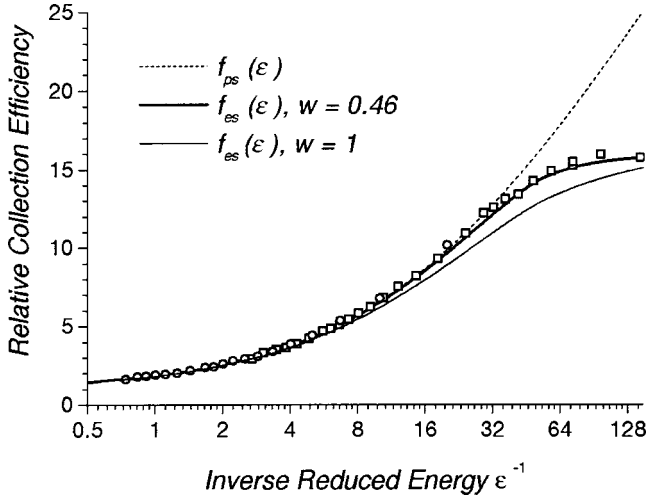

FIG. 4. Uncorrected [expression (4), dashed line] and corrected [expression (6), solid lines for two different Gaussian-shape beam profiles] relative collection efficiencies for the linear TOF apparatus with a floatable drift tube (dimensionless parameters: $k_0=0.15$; $k_1=4.2$; $k_2=0.068$) as a function of the inverse reduced energy $\epsilon^{-1}=|qU/E|$ The simulation results for one of the assumed beam profiles ($w=0.46$) and two different tube voltages are also shown by symbols [(□) $U=2900$ V; (○) $U=800$ V].

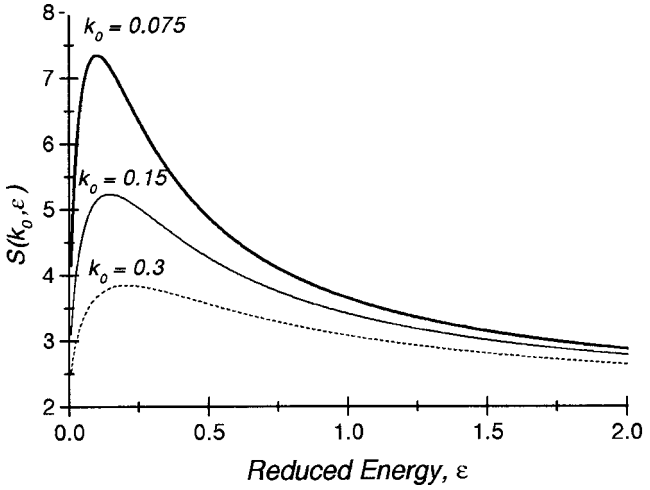

FIG. 5. Ratio of the relative energy to time-of-flight errors $S(\epsilon,k_0)=(\Delta E/E)/(\Delta t/t)$ as a function of reduced energy $\epsilon=|E/qU|$ for different values of the apparatus parameter $k_0=l/L$ [expression (7)].

Expression (7) depends now explicitly on the reduced energy of the analyzed particles as well as on the analyzer geometry illustrated in Fig. 5. This places an additional constraint on the accuracy of the TOF measurements, since an error in flight time will now result not only in an incorrect value for the particle energy, but may have an impact on the shape of the energy distribution as well. It is important to note also that peak width comparisons (for example, of binary collision peaks for neutrals and ions in large-angle scattering experiments) have to be made with caution, since the same intrinsic experimental flight time uncertainty Δt, arising from finite beam size and impact time distribution, will result after the TOF-to-energy transformation in different peak broadenings, ΔE, which depend on the mean peak reduced energy ϵ [see expression (7)].

III. EXPERIMENTAL APPROACH

A linear TOF system 75 cm long with a floatable drift tube ($k_0=0.148$; $k_1=4.2$; $k_2=0.068$) and a dual microchannel plate detector are implemented in the recently developed apparatus (Fig. 6) for low energy multicharged ion–surface interaction studies at the Oak Ridge National Laboratory (ORNL) Multicharged Ion Research Facility. Since the focus of this article is on TOF measurements performed using this apparatus, only a brief description of the entire setup is presented here. Additional details about the apparatus can be found in another publication.[11] Ions are extracted from an electron cyclotron resonance (ECR) ion source at 10 kV extraction voltage and decelerated to the desired energy in a floating ultrahigh vacuum (UHV) scattering chamber. Beam deceleration is accomplished by a six element zoom lens whose 2 mm diam exit aperture is located 2.5 cm upstream of the target at the center of the chamber. The beam spot on target can be determined by monitoring the current transmitted through a narrow slit on a beam stop translated immediately in front of the target. Typical spot sizes were measured to be 2–3 mm full width at half maximum (FWHM). In the present configuration the TOF system is oriented 120° with respect to the incident beam. The gold target used in the present experiment was prepared *in situ* by repeated cycles of Ar^+ sputtering and subsequent annealing for several minutes at about 450 °C. The target is attached to a sample mount positioned on an $x-y-z$ manipulator, permitting rotation about an axis perpendicular to the incident beam. The pressure in the scattering chamber was less than 3×10^{-10} mbar.

To permit TOF analysis, a beam chopping system was installed about 2 m upstream of the 90° deflector and is capable of producing ion pulses as short as 15–30 ns in

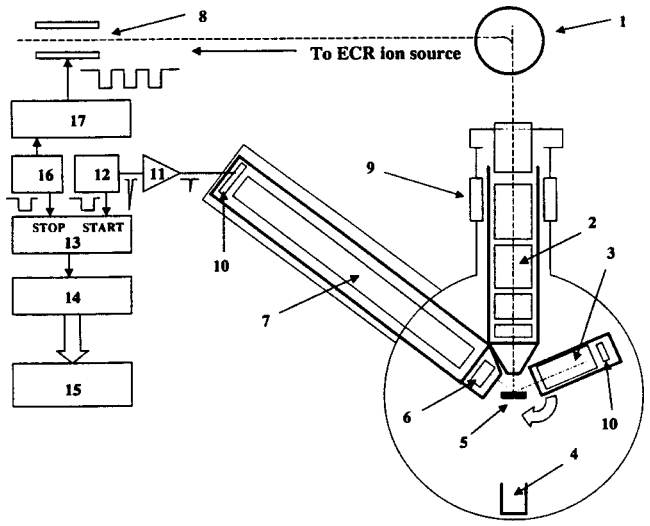

FIG. 6. Schematic of the experimental apparatus and TOF electronics: 1—90° spherical sector electrostatic deflector; 2—6-element deceleration zoom lens; 3—180° spherical sector electron spectrometer; 4—straight through Faraday cup; 5—sample; 6—electron impact ionizer; 7—biasable drift tube of the TOF analyzer; 8—beam chopping plates; 9—high voltage (HV) isolation to 15 kV; 10—dual microchannel plate detector; 11—fast amplifier; 12—constant fraction discriminator; 13—time-to-amplitude converter; 14—analog-to-digital converter; 15—computer; 16—low-amplitude function generator; 17—pulsed power supply.

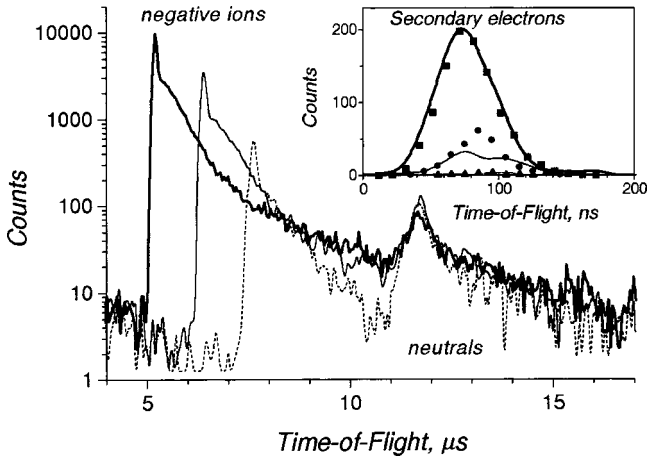

FIG. 7. TOF spectra acquired at three different drift tube voltages for the case of 590 eV O^{1+} projectiles incident on Au(110) 50° relative to the surface normal. Inset: Expanded region of the spectra at short flight times showing the secondary electron TOF peaks together with simulation results (shown by symbols). Thick lines (squares): $U=2900$ V; thin line (circles); $U=1500$ V; dashed line (triangles): $U=800$ V.

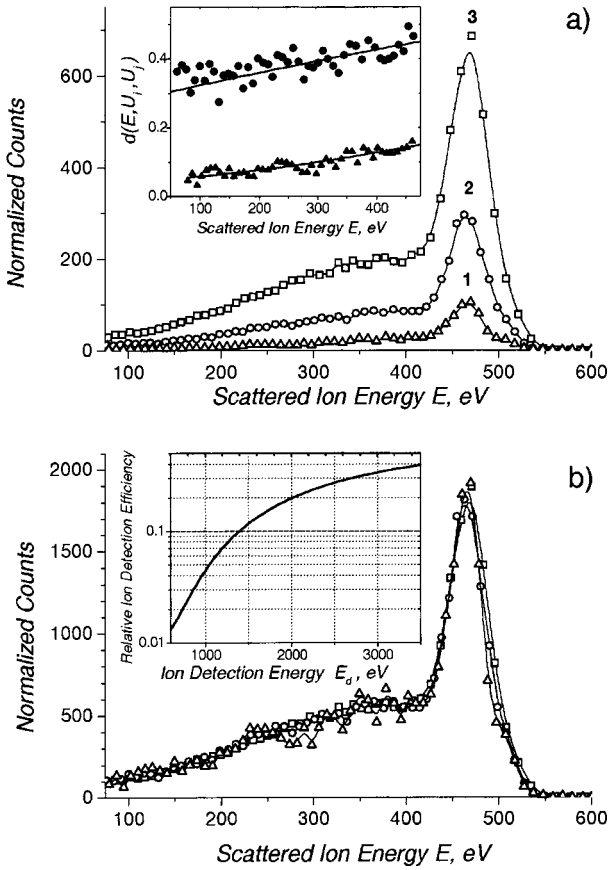

FIG. 8. (a) Results of TOF-to-energy transformations for the negative ion components of the spectra shown in Fig. 7 after corrections for (a) collection efficiency only and (b) detection efficiency as well: (□) $U=2900$ V; (○) $=1500$ V; (△) $U=800$ V. Inset (a) Ratios between curves 3 and 1, (▲) and curves 2 and 1, (●) shown together with results of the best fit (lines) calculated using expression (8) with parameters $a=2$, $b=1680$, $c=0.0095$, const$=1$. Inset (b) Relative ion detection efficiency [expression (8)], used in TOF-to-energy transformations, as a function of ion detection energy E_d for the parameters given.

width by periodically sweeping a beam of ions across a small aperture. The theory on obtaining such a short burst of ions from an ion beam is well developed[12] and the technique is widely used.[3,4,6] The scattered particle signal from the detector is used to trigger the time measuring cycle, while a sync pulse from the chopper stops the measurement. By accumulating a large number of such cycles, a TOF spectrum is produced. In all the measurements presented below, the detection rates did not exceed several kHz. This was much less than the typical chopper repetition rate ($\leqslant$50 kHz) chosen to accommodate a maximum flight time of 20 μs, so no dead time corrections[13] were needed for the TOF spectra acquired.

The obvious drawback of such a technique is the impossibility of direct determination of the impact time (i.e., time zero). This is typically not a problem in small-angle scattering experiments where detection of a part of the direct beam provides the necessary reference for energy loss analysis, but this is evidently not an option in a large angle scattering geometry. Several other techniques can be used to determine time zero in the TOF spectrum. The most direct method is detection of photons produced in the interaction by the same TOF detector. This provides immediate information about the impact time distribution, but is usually possible only in the case of multiply charged ion impact on surfaces where the photon number and energy generated are sufficient to overcome the usually low photon detection efficiency of commonly used microchannel plate detectors. Another method is secondary electron detection (where possible), which is more efficient but requires additional information about the electron energy distribution for accurate determination of time zero. Alternatively, an auxiliary detector (such as an electron spectrometer in our case) can be used to detect photons or electrons produced during the interaction (the difference in internal time delays of the detection channels has to be taken into account in this case). Finally, an important issue for TOF measurements is an accurate time calibration. An ORTEC 462 time calibrator was used in the present case. It permits calibration of time periods from 10 ns to 80 μs and has an absolute accuracy $\pm$10 ps for a 10 ns period.

IV. RESULTS AND DISCUSSION

Selected data for the case of scattering O^{1+} ions from a Au(110) single crystal surface are presented here to illustrate the type of information which can be gained using a TOF analyzer with a floatable drift tube. The measurements were performed for incidence angles spanning the range of 0°–50° (relative to the surface normal) and at a ''random'' azimuth direction, with the drift tube biased positively to analyze negative ion and neutral fractions. The ORIGIN 5.0 software package and in-house developed computer codes for TOF spectrum simulations and TOF-to-energy transformations were used for data analysis.

A. Relative ion detection efficiency

Figure 7 shows TOF spectra acquired at three different drift tube voltages for a case of 590 eV O^{1+} projectiles incident on Au(110) at 50° relative to the surface normal. Expanded regions of the spectra at short flight times that show the secondary electron peaks are presented in the inset. A

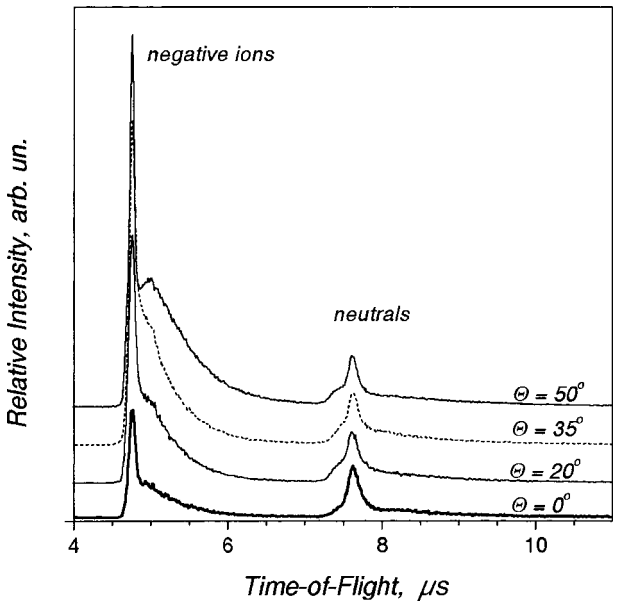

FIG. 9. Backscattered projectile TOF spectra for 1.4 keV O^{1+} ions incident on Au(110) over a range of angles.

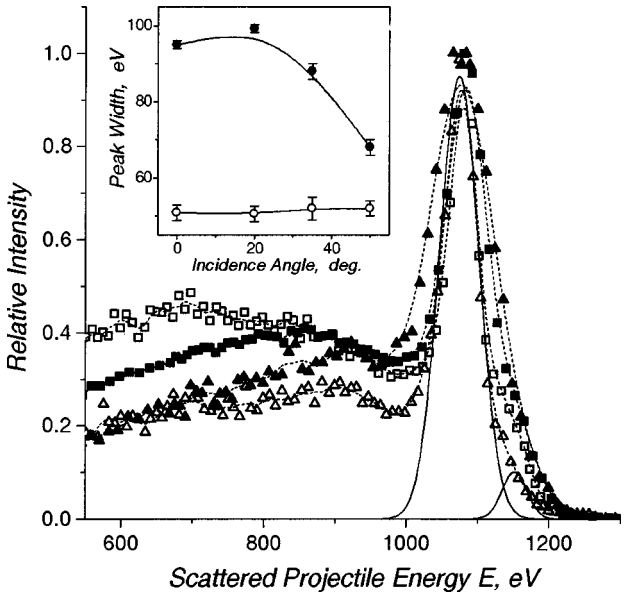

FIG. 10. Results of TOF-to-energy transformations of the spectra shown in Fig. 9 for 0° [(△) for neutrals, (▲) for ions] and 50° (squares) incidence angles (relative to the surface normal). Curves are normalized to the maxima of the binary collision peaks. Fit of the neutral binary collision peak with two Gaussian distributions for 0° incident angle is also shown as solid lines. Inset: Widths of the Gaussian fits to the neutral (○) and negative ion (●) binary collision peaks over the entire range of incidence angles.

low negative voltage $u=-4.2$ V was applied to one of the grids in front of the drift tube to prevent very slow electrons from broadening the peak. All detector voltages were kept constant in relation to the drift tube voltage to ensure the same detection conditions (i.e., the same electric fields in front of the detector and inside the microchannels which define secondary electron trajectories and affect the detector output signal). The potential difference applied between the first microchannel plate and the drift tube exit grid was kept negative ($\Delta V=-200$ V), mainly to prevent detection of secondary electrons produced in the drift tube by particle collisions with the tube walls.

Both the negative ion and neutral parts of the spectra consist of comparatively sharp peaks very close in position to that expected for binary collisions between the incident projectiles and isolated Au atoms, and long straggling tails resulting from multiple collisions. A significant drop in the number of detected ions with decreasing drift tube voltage is clearly discernible. The time zero reference needed for the TOF-to-energy transformation was obtained by fitting the measured electron TOF peaks with a simulation that incorporated finite beam size and start-time spread and that was based on a secondary electron energy spectrum (not shown) acquired with the electron spectrometer. The simulation results are shown in the inset by symbols. It can be seen from the inset that the electron TOF peak is practically gone at the lowest tube voltage applied. This can be attributed to the influence of the residual (Earth's) magnetic field (note that the detection efficiency for 600 eV electrons is comparable or might even be higher than that for 1.3 and 2.7 keV electrons due to the energy dependence of the electron-induced secondary electron emission). A simulation of the dependence of the peak amplitude on the drift tube voltage provides an estimate of the transverse field strength of ~0.1 G, which is sufficiently low to not significantly affect the ion trajectories.

Figure 8(a) shows the results of the TOF-to-energy transformation for the negative ion components of the spectra after correction for collection efficiency [see expression (6) and Fig. 4]. Figure 8 illustrates the effect of tube voltage on ion detection efficiency, as well as the procedure used for making the required correction. To that end, in the inset of Fig. 8(a) ratios between measured scattered ion energy distributions acquired at different tube voltages are shown. These ratios correspond precisely in form to those required in expression (1),

$$d(E',U',U'')=\frac{D[E'+|q(U'-\Delta V)|]}{D[E'+|q(U''-\Delta V)|]}=\frac{D(E+|qU|)}{D(E)},$$

where $E=E'+|q(U''-\Delta V)|$ and $U=U'-U''$.

As described in Sec. I, by making auxiliary measurements at scattered ion energy E' with two appropriate drift tube voltages, the ratio of detection efficiencies required for ion fraction estimates is determined. Even though not required for ion fraction determinations *per se*, the functional form of $D(E_d)$ (i.e., the dependence on detection energy) can be deduced as well, which is of interest in other applications. From inspection of a large set of measurements taken at constant scattered ion energy E but with different tube voltages, the following analytical form describing the dependence of detector efficiency on ion detection energy $E_d=E+|q(U-\Delta V)|$ was deduced:

$$D(E_d)=\text{const}\left[\left(\frac{E_d-a}{E_d}\right)^b+c\right], \tag{8}$$

with parameters a, b, and c determined by a manual fitting procedure. The quality of the fit was checked by a least squares comparison of calculated values $d(E,U_i,U_j)$, where

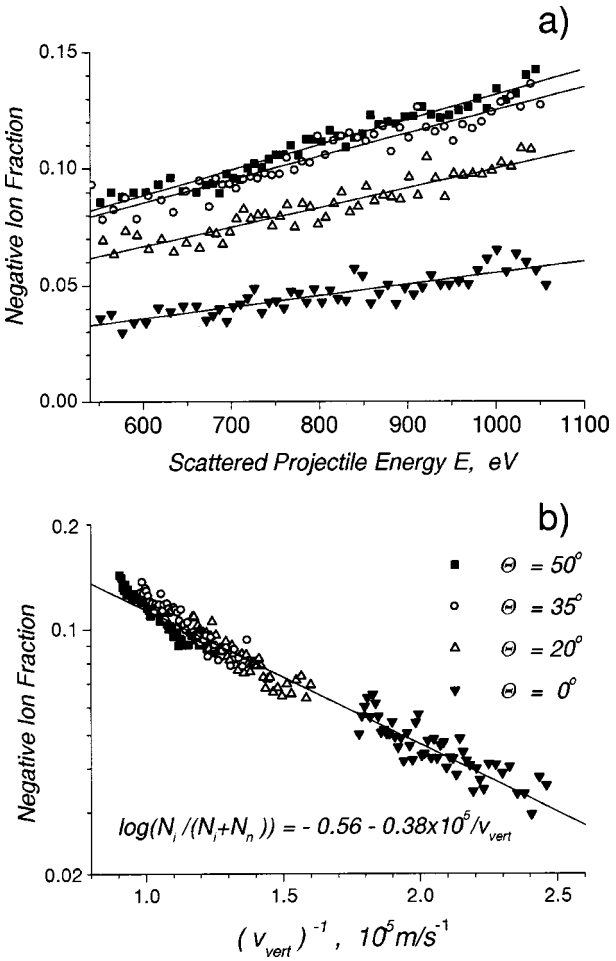

FIG. 11. Negative ion fraction (obtained from the TOF spectra shown in Fig. 9) as a function of the (a) scattered projectile energy and (b) inverse vertical velocity. The lines are linear fits to the data.

U_i and U_j are different drift tube voltages, with the measured ratios shown in the inset of Fig. 8(a) (the result of the final fit is shown by lines). Since in the present instance the measurements were not normalized to the absolute particle flux entering the analyzer, only the energy dependence could be found from our experiments [i.e., the const in expression (8) was arbitrarily set equal to unity]. Figure 8(b) shows the results of TOF-to-energy transformations taking into account the thus deduced ion detection efficiency which is reproduced in the inset of Fig. 8(b).

B. Ion fraction measurements

Figure 9 shows TOF spectra for the case of 1.4 keV O^{1+} projectiles incident on Au(110) over a range of angles and Fig. 10 presents the results of TOF-to-energy transformations for 0° (open triangles for neutrals and closed triangles for ions) and 50° (squares) incident angles (relative to the surface normal). As can be seen in Fig. 10, the widths of the neutral binary collision peaks remain practically the same (the difference being in the broadening on the high energy sides of the peaks that can be attributed to double scattering events leading to the same final deflection with lower total energy loss), while the widths of the corresponding negative ion peaks are broader and depend on the incident angle. In the inset of Fig. 10 the corresponding widths for all four measured incident angles are presented; they were obtained by fitting the peaks with two Gaussian distributions using the ORIGIN nonlinear fitting tool, and are shown in Fig. 10 by solid lines. The width difference between neutrals and ions cannot be ascribed to any apparatus effect. Any systematic errors will result in a flight time uncertainty which in turn causes energy distribution peak broadening. According to expression (7) this broadening can be different for ions and neutrals [since corresponding slopes for dependence $\Delta E(\Delta t)$ are different], but, if the neutral peak width remains the same, the ion peak width should exhibit the same tendency. The width differences might alternatively be attributable to differences in trajectories leading to neutral atom or negative ion formation. The binary collision approximation is certainly an idealization of the real interaction, which might be sufficient to describe elastic energy losses, but may fail in the presence of inelastic loss. We defer in the present article further discussion of the issue of differing binary peak widths, and present below negative ion fractions only for the straggling tails of the distributions resulting from multiple collisions. In addition to avoiding the elastic peaks, focus on the straggling tails assures that charge equilibration has occurred prior to negative ion formation on the exit trajectory. In addition, the negative ion fraction in this case is given simply by expression (1), since for oxygen projectiles positive ions can survive only in binary collisions.[11]

Figure 11 shows the negative ion fraction as a function of scattered particle energy and inverse vertical velocity. As can be seen in the lower plot of Fig. 11, the negative ion fraction coalesces, within experimental errors, into a single curve when plotted as function of inverse vertical velocity that decreases quite steeply with increasing $1/\nu\perp$. The former feature suggests that the determinant parameter of negative ion formation for our geometry and conditions is the time the scattered projectile spends near the surface on its exit trajectory. Such behavior has been previously observed by van Wunnik *et al.*[14] who investigated H^- formation during large-angle scattering from cesiated W surfaces. van Wunnik *et al.* found that, while a strong parallel velocity dependence was evident for Cs coverages resulting in the lowest surface work functions (closest in resonance to the H^- affinity level), for lower Cs coverages and correspondingly larger surface work functions, the dominant dependence below the H^- maximum was on perpendicular velocity. Further measurements are planned to determine if the observed behavior is typical of the negative ion formation in other species as well.

ACKNOWLEDGMENTS

This research was sponsored in part by the Office of Fusion Sciences, and by the Office of Basic Energy Sciences of the U.S. Department of Energy under Contract No. DE-AC05-96OR22464 with Lockheed Martin Energy Research Corp. One of the authors (V.A.M.) was appointed through the ORNL Postdoctoral Research Associates Program administered jointly by ORISE and ORNL.

[1] D. Ioanoviciu, Int. J. Mass Spectrom. Ion Processes **131**, 43 (1994).
[2] B. T. Chait and S. B. H. Kent, Science **257**, 1885 (1992).
[3] O. Grizzi, M. Shi, H. Bu, and J. W. Rabalais, Rev. Sci. Instrum. **61**, 740 (1990); D. Y. Dubrovitskii, A. P. Kalinin, and V. A. Morozov, Instrum. Exp. Tech. **39**, 238 (1996).
[4] V. A. Morozov, F. W. Meyer, and P. Roncin, Phys. Scr. **T80**, 69 (1999).
[5] J. L. Shinpaugh, F. W. Meyer, and S. Datz, Nucl. Instrum. Methods Phys. Res. B **99**, 198 (1995); I. G. Hughes, V. Morozov, B. Merron, J. Boyle, J. Rainnie, I. D. Williams, and R. J. H. Davies, Rapid Commun. Mass Spectrom. **11**, 1509 (1997).
[6] B. Willderding, H. Steininger, K. J. Snowdon, and W. Heiland, Nucl. Instrum. Methods Phys. Res. B **2**, 453 (1984).
[7] M. Maazouz, L. Guillemot, T. Schlatholter, S. Ustaze, and V. A. Esaulov, Nucl. Instrum. Methods Phys. Res. B **125**, 283 (1997).
[8] J. N. Chen, M. Shi, and J. W. Rabalais, J. Chem. Phys. **86**, 2403 (1987).
[9] H. Winter, Phys. Rev. A **46**, R13 (1992).
[10] J. N. M. van Wunnik, J. J. C. Geerlings, E. H. A. Granneman, and J. Los, Surf. Sci. **131**, 17 (1983).
[11] F. W. Meyer and V. A. Morozov, Nucl. Instrum. Methods Phys. Res. B **157**, 297 (1999).
[12] T. K. Fowler and W. M. Good, Nucl. Instrum. Methods **7**, 245 (1960).
[13] F. Esposito, N. Spinelli, R. Velotta, and V. Berardi, Rev. Sci. Instrum. **62**, 2822 (1991); P. B. Coates, *ibid*. **63**, 2084 (1992).
[14] J. N. M. van Wunnik, J. J. C. Geerlings, and J. Los, Surf. Sci. **131**, 1 (1983).